Olivier Pinel, Mahdi Hosseini, Ben M. Sparkes, Jesse L. Everett, Daniel Higginbottom, Geoff T. Campbell, Ping Koy Lam, Ben C. Buchler
Gradient echo quantum memory in warm atomic vapor
Jove-Journal of Visualized Experiments, 2013; (81):e50552-1-e50552-10

Originally published at:
http://doi.org/10.3791/50552

Video Article

Gradient Echo Quantum Memory in Warm Atomic Vapor

Olivier Pinel[1], Mahdi Hosseini[1], Ben M. Sparkes[1], Jesse L. Everett[1], Daniel Higginbottom[1], Geoff T. Campbell[1], Ping Koy Lam[1], Ben C. Buchler[1]

[1]ARC Centre for Quantum Computation and Communication Technology, Department of Quantum Science, The Australian National University

Correspondence to: Ben C. Buchler at ben.buchler@anu.edu.au

URL: http://www.jove.com/video/50552
DOI: doi:10.3791/50552

Keywords: Physics, Issue 81, quantum memory, photon echo, rubidium vapor, gas cell, optical memory, gradient echo memory (GEM)

Date Published: 11/11/2013

Citation: Pinel, O., Hosseini, M., Sparkes, B.M., Everett, J.L., Higginbottom, D., Campbell, G.T., Lam, P.K., Buchler, B.C. Gradient Echo Quantum Memory in Warm Atomic Vapor. *J. Vis. Exp.* (81), e50552, doi:10.3791/50552 (2013).

Abstract

Gradient echo memory (GEM) is a protocol for storing optical quantum states of light in atomic ensembles. The primary motivation for such a technology is that quantum key distribution (QKD), which uses Heisenberg uncertainty to guarantee security of cryptographic keys, is limited in transmission distance. The development of a quantum repeater is a possible path to extend QKD range, but a repeater will need a quantum memory. In our experiments we use a gas of rubidium 87 vapor that is contained in a warm gas cell. This makes the scheme particularly simple. It is also a highly versatile scheme that enables in-memory refinement of the stored state, such as frequency shifting and bandwidth manipulation. The basis of the GEM protocol is to absorb the light into an ensemble of atoms that has been prepared in a magnetic field gradient. The reversal of this gradient leads to rephasing of the atomic polarization and thus recall of the stored optical state. We will outline how we prepare the atoms and this gradient and also describe some of the pitfalls that need to be avoided, in particular four-wave mixing, which can give rise to optical gain.

Video Link

The video component of this article can be found at http://www.jove.com/video/50552/

Introduction

One of the outstanding challenges facing quantum information technology is the ability to build a memory for quantum states. For photonic quantum computing [1], or a quantum repeater used in a quantum key distribution system [2], this means building a memory that can store quantum states of light [3]. One of the approaches taken towards this goal is to use ensembles of atoms that can be controlled in such a way as to store and then controllably release light at some later time. Numerous techniques have been developed including electromagnetically induced transparency (EIT) [4], the atomic frequency comb (AFC) [5, 6, 7], four-wave mixing (FWM) [8], Raman absorption [9], Faraday interaction [10] and photon echo techniques [11, 12, 13, 14, 13, 15, 16, 17, 18, 19].

The focus of this paper is Λ - Gradient Echo Memory (Λ -GEM), which works using three-level 'Λ' structured atomic media. It was initially implemented in a warm Rb vapor cell in 2008 [20]. This scheme has been used as a random access memory for light pulses, [21], has a demonstrated efficiency as high as 87% [22], provides noiseless storage of quantum states [23] and shows some promise as a platform for nonlinear optical operations [24]. We have also recently published a paper that goes into some detail about the interaction of this memory with warm atomic vapor [25].

The essence of the technique is that we prepare an ensemble of atoms that is inhomogeneously broadened so that the atoms will absorb a pulse of light. In our experiment we use Raman absorption, as shown in **Figure 1a**. The probe light, which is to be stored, will be mapped onto the coherence between two ground states of the atoms. The broadening is provided by applying a magnetic field gradient along the direction of optical propagation, inducing a spatial gradient in the Raman absorption frequencies, as shown in **Figure 1b**. The different frequency components of the stored pulse are thus mapped to different spatial locations linearly along the length of the atomic ensemble. In other words, the spatial profile of the atomic spin wave that is generated by the absorption of the input pulse is proportional to the Fourier transform of the temporal profile of the input pulse. As we will outline later, it is this frequency gradient that also enables some of the interesting spectral processing capabilities of this memory. By reversing the field gradient, the evolution of the coherence of the atomic ensemble can be time-reversed. This allows for the retrieval of the pulse of light.

Protocol

1. Some Custom-built Elements

1. **Ring resonators**
   In this experiment, two ring resonators that split and combine beams of different frequencies are required. The design of the cavity is shown in **Fig. 2**.

1. Build the resonators around a hollowed cylinder of bulk aluminum. On one end, mount two flat mirrors with identical reflectivity. On the opposite end mount a maximum reflectivity curved mirror. The mirrors do not need to be glued to the cavity spacer. With careful machining of the spacer, the end-caps are enough to hold them in place.
2. Combine the curved mirror with an O-ring and piezoelectric actuator to allow control of the cavity resonance frequency. Place the O-ring between the mirror and the cavity spacer, with the piezo behind the mirror. Compress these elements onto the cavity spacer with the end-cap to allow for fast actuation of the end mirror. The combination of O-ring compression and high-speed piezo typically allow for control bandwidths in excess of 10 kHz.
   Note: For this example, the spacers are about 25 cm long. This length is arbitrary, although it should be chosen so that the control and probe light are not coresonant, which means that the hyperfine splitting must not be a multiple of the free-spectral-range. Due to the ring geometry, the cavity will have nondegenerate polarization modes of different finesse. The custom coated mirrors are specified to provide a cavity of finesse around 1,000 for s-polarized light, which leads to a finesse of around 100 for p-polarized light. While these experiments are typically conducted on the low-finesse mode, the setup could easily be switched to the high-finesse mode should stronger filtering of the beams be required.

2. **Design of the memory cell and its housing**
   1. To build the memory apparatus, use a long cell containing isotopically enhanced ^{87}Rb along with 0.5 Torr of Kr buffer gas. In the setup, the length is 20 cm. The windows of the cell are antireflection coated. This cell must be heated to around 80 °C using a nonmagnetic heating wire.
   2. Encase the cell in three concentric solenoids. The two inner solenoids create the magnetic field gradients. To wind these solenoids, perform a simulation using the Biot-Savart equation. Simulate the variable-pitch solenoid that will provide a linearly varying magnetic field.
   3. Using a graphing program, print out a plot of this spiral onto a piece of paper. Wrap the paper around a PVC pipe to provide a line to follow and wind the wire onto the pipe.
      Note: In this setup the coils are 50 cm long, over twice the length of the gas cell, to avoid edge effects. The diameters are 6 and 10 cm, which is twice the diameter of the cell, to ensure the magnetic fields are mostly longitudinal. The gradient solenoids oppose each other so that switching between them will switch the sign of the gradient (see **Fig. 3**). In a typical experiment, 2-3 A of current is run through these coils and the coils are switched in 3-4 µsec.
   4. To optimize the switching time and stop oscillations use 200 Ω damping resistors in series with the coils. Place these two solenoids inside the third normally wound coil that is used to provide a DC magnetic field to lift the degeneracy of the Zeeman levels. Rubidium has a shift of about 1.4 MHz/G of magnetic field [26]. A typical DC field is 6 G, while the gradients would be 2 G/m.
   5. Place two layers of µ-metal shielding around the three magnetic coils to reduce the influence of the Earth's magnetic field on the experiment.

2. Layout of the Optical Beam Path

1. Use a single mode laser tuned near the rubidium D_1 line at 795 nm. Monitor the frequency of the laser using a saturated absorption measurement, as shown in **Figure 3**. Detune the frequency by about 1.5 GHz above the F=2 to F'=2 transition. This will be the approximate frequency of the control beam.
2. At the beamsplitter BS2, tap some light off the main laser to form the control beam. Shift its frequency by using the acousto-optic modulator AOM1. This AOM also allows modulation of the control beam power. To drive the AOM, pass the output of a signal source through an RF switch that is controlled by a TTL signal, and then amplify the signal before sending it into the AOM. Fine tune the control frequency, to optimize the Raman absorption for example, by changing the drive frequency of this AOM. The RF drive frequency of the AOMs in the setup is 80 MHz, but this is arbitrary.
3. Detune the probe beam, which will be stored in the quantum memory, by 6.8 GHz from the control beam, this frequency being the hyperfine ground state splitting of ^{87}Rb. To prepare this frequency, pass the laser through a fiber-coupled electro-optic modulator that is driven by a 6.8 GHz microwave source. This generates an array of sidebands at harmonics of 6.8 GHz, above and below the carrier frequency.
4. To obtain a probe beam with a pure frequency, separate the +6.8 GHz light from all the other unwanted modulation sidebands. To do this, use one of the ring cavities. Lock Cavity 1 on resonance with the +6.8 GHz sideband. This frequency will then be transmitted through the resonator, while all other frequencies are reflected, thus preparing a pure frequency that will address the F=1 ground state of the rubidium atoms. The cavity may be locked using the Pound-Drever-Hall technique [27], using the light reflected from the input mirror.
5. Tap off a part of the laser beam at BS3 and send it through AOM2 to allow fine control of the frequency and intensity of the probe beam. There are a couple of methods available to drive the AOM. For instance, use a programmable signal generator set to generate Gaussian pulses modulated at 80 MHz. Alternatively, combine a continuous 80 MHz signal with a pulse at an RF mixer to give a pulse modulated at 80 MHz. Either way, this modulated Gaussian is then amplified and sent into the AOM to give a pulse of light into a diffracted order of the AOM.
   Note: This diffracted order will provide finely controlled pulses of light that can be stored in the memory. The amplitude of the pulses can be tuned using a combination of the AOM drive power and varying the splitting ratio of BS1. This allows reliable production of a wide range of pulse amplitudes, and in particular, allows the production of very weak pulses with mean photon numbers less than 1 [23].
6. The next stage is to recombine the probe and control beams. This could be done with a simple beamsplitter, but that would mean losing some portion of the light. If the polarization of the probe and control were orthogonal then lossless recombination could be achieved using a polarizing beam splitter, but the storage can only truly be optimized via independent control of the probe and control polarizations.
   1. To achieve this, use a second, high-efficiency, impedance-matched, ring cavity. Set up a cavity so that the probe beam is transmitted through, while the control field is reflected off the output mirror. Transmission of the probe through this second resonator also provides a second layer of frequency filtering, which helps avoid problems with four-wave mixing.
   2. Lock this cavity to the frequency of the probe beam using an auxiliary locking beam (dashed line) that is injected into the reverse mode of the cavity. Tune this beam to a different frequency, polarization and spatial mode from the probe beam so that it may be detected on reflection without adversely affecting the probe beam. The reason for this effort is that it is fiendishly difficult to use the low-power, pulsed probe beam to lock the cavity. The control and probe beams are collimated before the memory cell to 7 mm and 3 mm sizes, respectively.

3. The control field power before the memory cell is ~270 mW and probe power may be chosen from zero to a few microwatts depending on the experiment run. Using a quarter-wave plate, adjust the polarization of the combined probe and control beams to be (approximately) circular and of the same helicity. Inject them into the memory gas cell apparatus.

7. Control the timing of all the elements of the experiment using a LabVIEW program [28]. A typical duty cycle would be 120 µsec. Switch the heater off during the memory storage time to avoid interference with the memory operation. A typical timing sequence is shown in **Figure 4**. When possible, switch the control beam off while the light is stored in the memory. In a warm gas cell, although the Raman transition is detuned from the excited state beyond the Doppler width, the control field can still be a significant source of decoherence in the memory due to the non-zero probability of the spontaneous Raman scattering. The Raman scattering is directly proportional to the control field power and inversely to the detuning squared. If the control field is kept on during the entire storage time, it can interact with the two lower states and destroy the coherence with the exponential rate defined by the scattering. This is explained further in the discussion section.
8. After storage and recall, pass the probe through a filtering cell in order to strip the control field from the beam. It is possible to use a cell with a natural mixture of Rb. The ^{85}Rb dominates and absorbs strongly at the control beam frequency, providing 60 dB of suppression. The probe beam is attenuated much less, typically 1.4 dB. Use a cell 75 mm long, heated to 140 °C. A cell with isotopically enhanced ^{85}Rb would lead to less probe absorption.
9. The final step is the detection of the probe pulses, using a homodyne or heterodyne detection. The advantage of this detection method is that it is mode selective so some residual control light will not impact on the measurements. The echo has a (near) circular polarization that is made linear using a half-wave/quarter-wave plate combination.
    1. To produce the local oscillator, tap off a part of the beam at BS4 and shift its frequency using AOM4. Store the signal from the homodyne or heterodyne setup using a fast oscilloscope, triggered to the LabVIEW control program.

Representative Results

1. Using the Raman Absorption as a Diagnostic Tool

The first result to obtain is a Raman line absorption of the probe beam light. Optimization of this absorption feature goes a long way towards achieving the best memory performance. With the magnetic gradient coils switched off, the control frequency can be scanned in the presence of a weak continuous probe wave. The absorption of the probe beam is directly related to the optical density of the atomic cell. Based on that, the temperature of the cell, power of the control beam and single photon detuning can be optimized through an iterative process to give the best possible Raman absorption. Too much control-beam power will increase absorption, but also broaden the width of the line. When optimized, the width is of the order of 100 kHz in our system.

Switching on one of the gradient coils will broaden the Raman line. The width of the broadened absorption determines the bandwidth of the memory. A compromise then has to be made between optical density, which affects memory efficiency, and memory bandwidth. The probe transmission is shown for one of our broadened Raman lines in **Figure 5**, where the memory bandwidth is set to about 1 MHz.

Switching on both magnetic gradient coils at the same time, the nonbroadened absorption linewidth should be recovered. Any mismatch in the current magnitude or spatial inhomogeneity of the magnetic fields will reflect directly on a broadening and distortion of the Raman absorption.

2. Pulse Storage

The simplest configuration for the memory is single pulse storage and retrieval. That would be, for instance, storing pulses of duration 2 µsec and switching the magnetic gradient coils 3 µsec after the pulse peak, as shown in **Figure 6**. If the optical density is low, some light leakage will be observed depending on the optical density (OD) of the medium. Carefully tuning the memory parameters is essential to obtaining high efficiency storage. This includes the optimization of the memory cell temperature, the careful alignment between the probe and the control field, tuning the intensity of the control beam to find the best compromise between absorption and scattering, ensuring the correct polarization of the beams and tuning the frequencies of the probe and control beams. This optimization method is further explained in the discussion section. Efficiencies exceeding 80% for a storage time of 4 µsec [22] can be expected when all these parameters are tuned well. The efficiency of the storage is defined as the ratio between the energy of the recalled echo and the energy of an identical pulse that has not been stored in the memory. This effectively factors out the effect of linear losses, for instance due to Fresnel reflections on the surfaces or absorption in the filtering cell. When using a heterodyne detection, the energy of the pulses is measured by squaring the heterodyne signal and measuring the areas of the pulse's envelopes.

The frequency and bandwidth of the retrieved pulse depends on the current injected into the gradient coils. Simple manipulation of these currents allows for fine tuning of the retrieved pulse. More complex spectral manipulations (such as those outlined in [29]) can be done using a more advanced coil setup where the gradient along the memory can be tuned as a function of position and time independently.

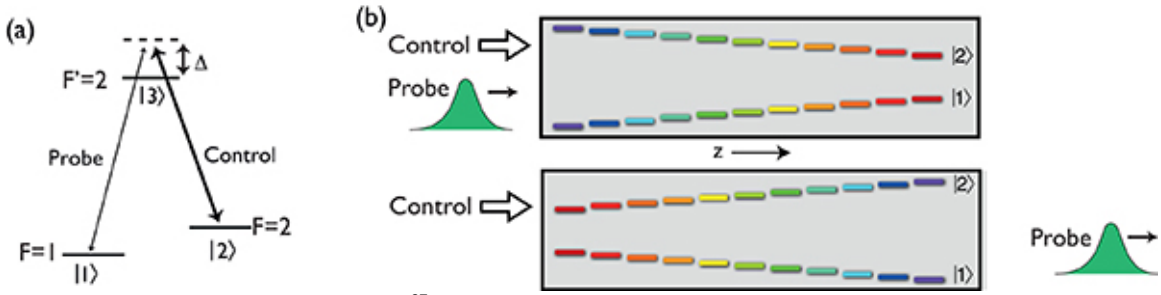

Figure 1. a) **The level scheme within the ^{87}Rb D_1 line used in the memory**. The probe light is Raman absorbed to create a coherence between the F=1 and F=2 ground-states. **b**) The magnetic field gradient gives spatially dependent detuning of the ground-states along the length of the cell. Reversing the gradient and turning the control beam on gives recall of the stored probe light. (Adapted from [34]). Click here to view larger image.

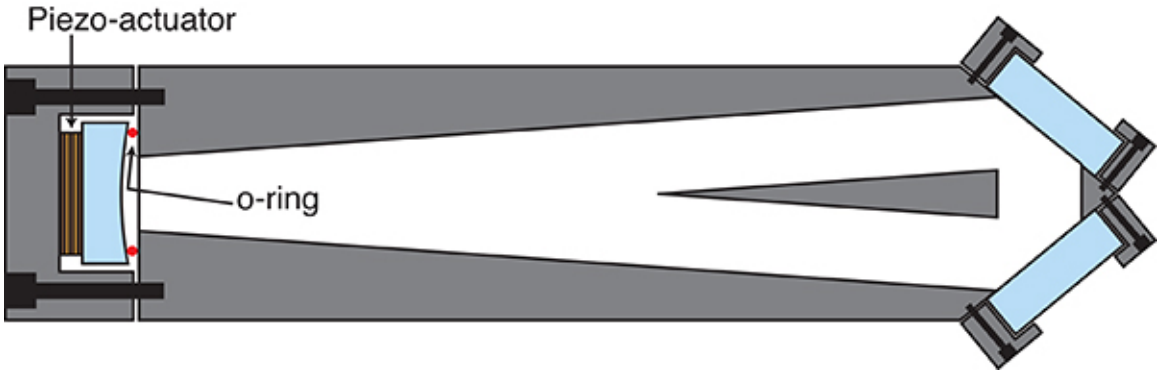

Figure 2. Schematic of an optical mode cleaner. Refer to the Methods section for a description. Click here to view larger image.

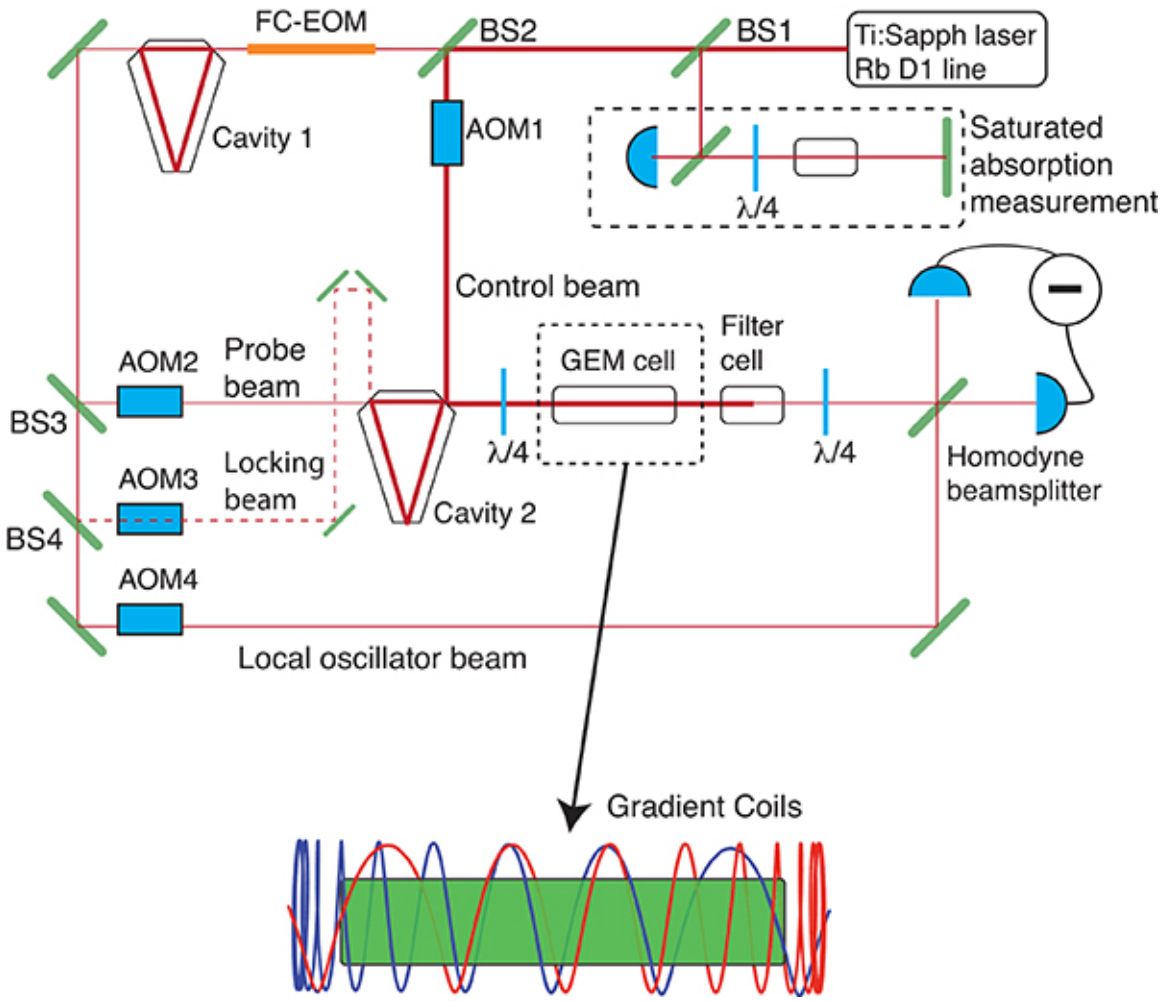

Figure 3. Schematic of the experimental setup. AOM = Acousto-Optic Modulator; EOM = Electro-Optic Modulator; BS=Beamsplitter; λ/4=Quarter-wave plate. Click here to view larger image.

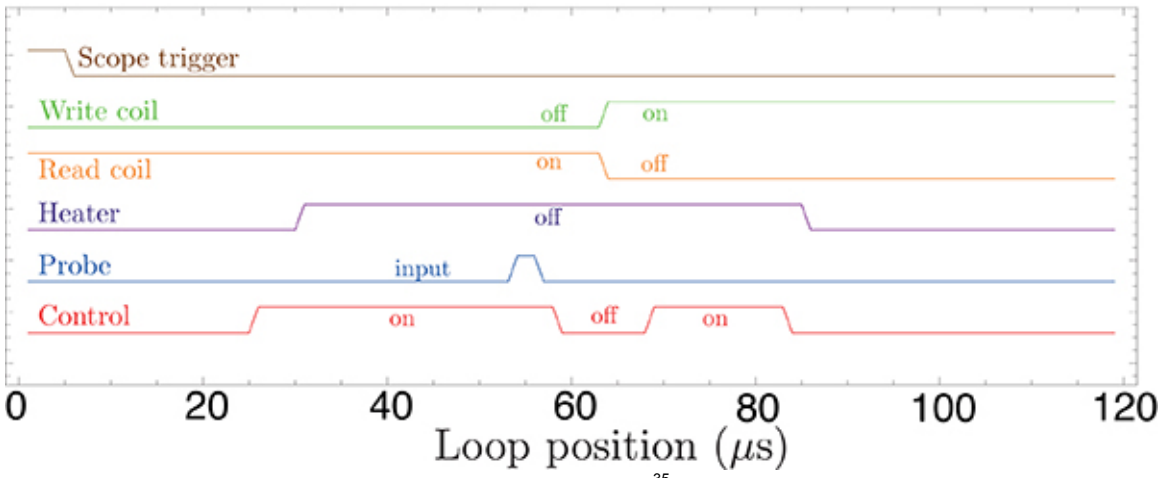

Figure 4. A typical timing sequence for the memory. (Taken from [35]). Click here to view larger image.

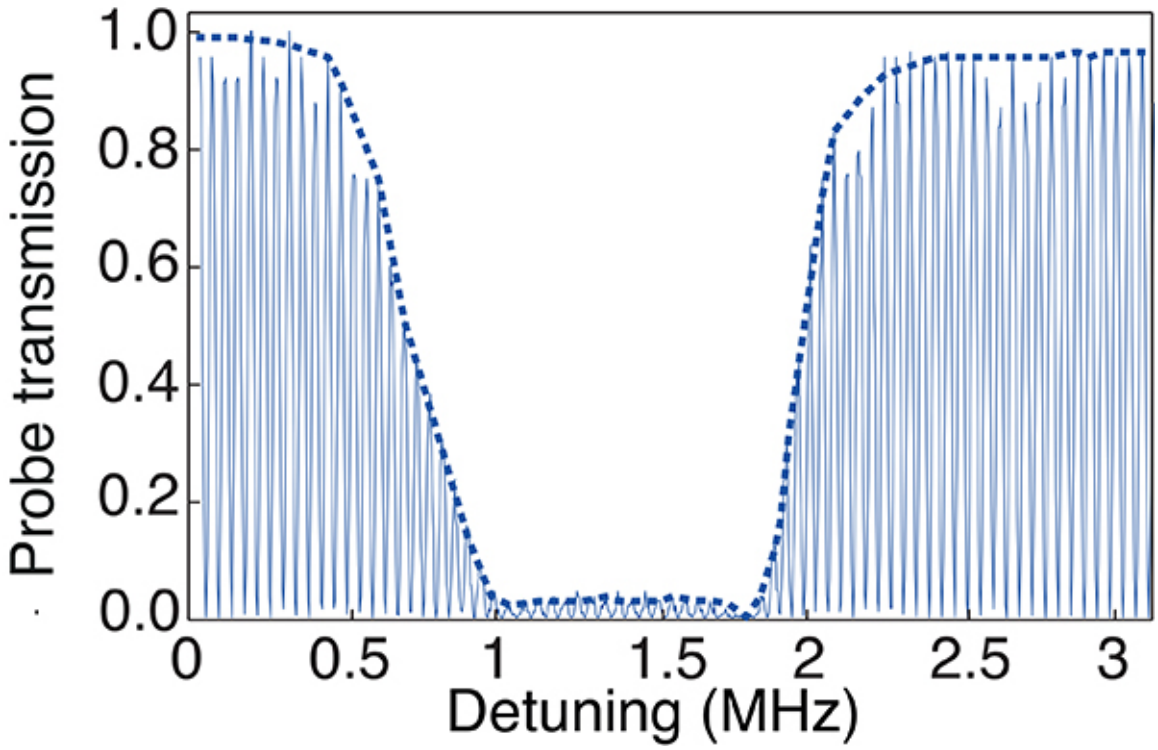

Figure 5. Typical heterodyned broadened Raman line when one of the magnetic gradient coils is switched on. The data (thin solid line) is taken using heterodyne measurement. The oscillation is due to the beat between the probe light and local oscillator light. The dashed curve shows the envelope of this data which is the shape of the broadened Raman line. (Modified from [25]). Click here to view larger image.

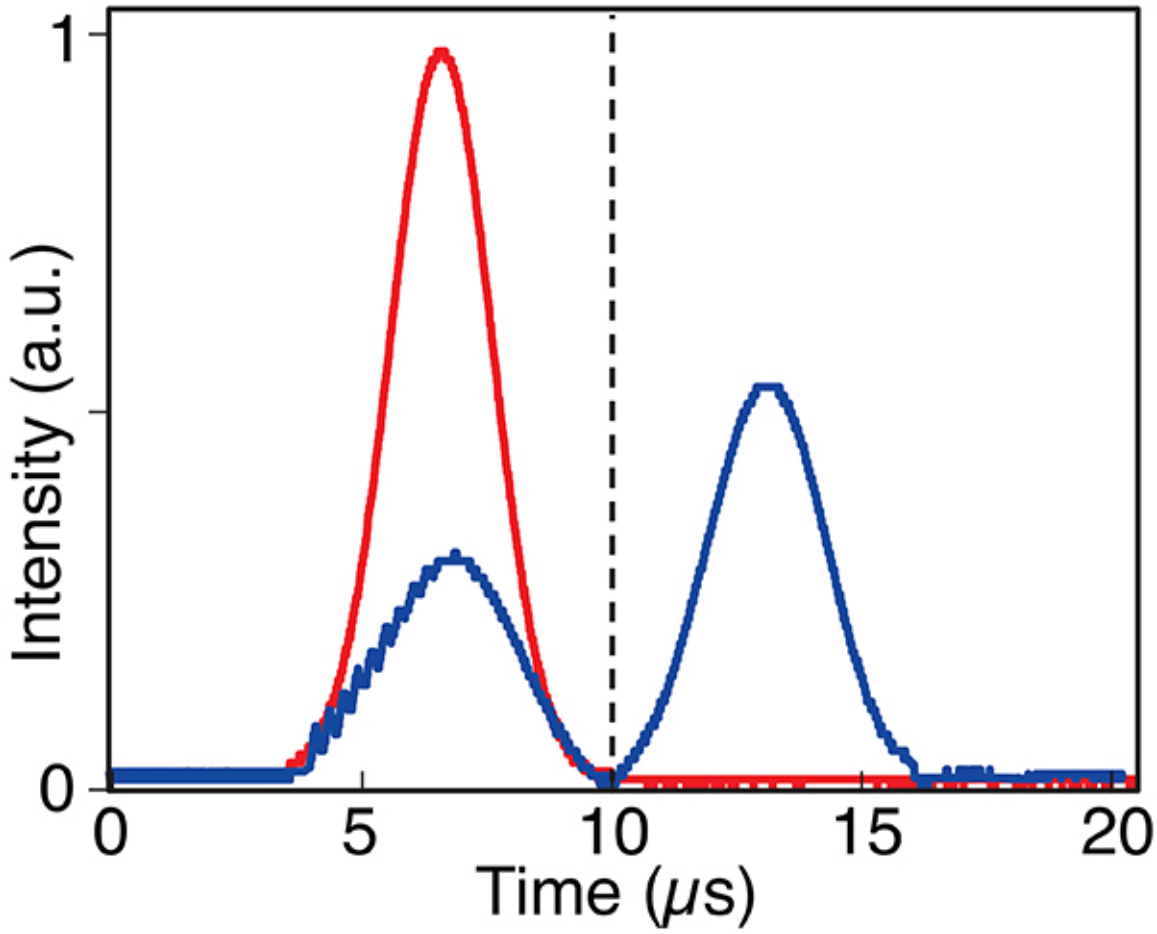

Figure 6. Typical average-efficiency GEM echo for short storage time. The magnetic gradient coils are switched at t = 10 μsec (dashed line). Red: input pulse intensity profile. Blue: intensity output of the memory, demonstrating leaked light (which is apparent under the red input pulse) and recalled echo, which appears to the right of the dashed line. Click here to view larger image.

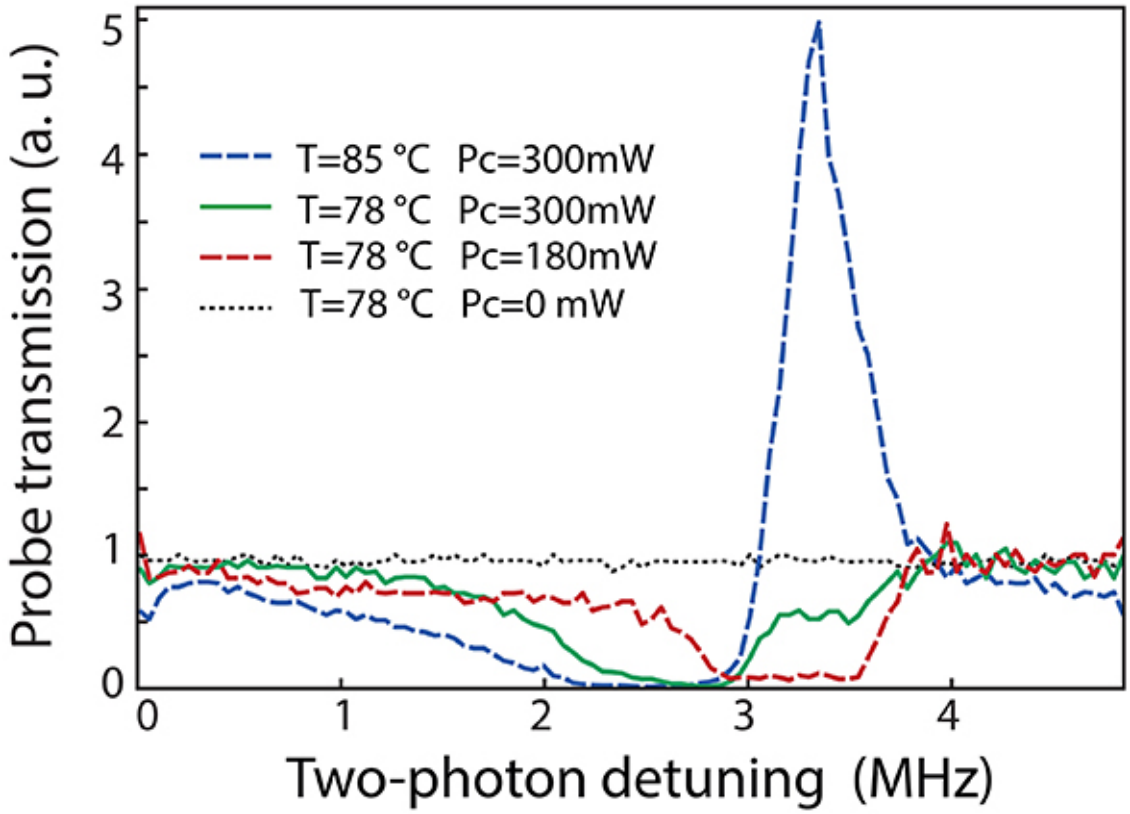

Figure 7. Four-wave mixing effect, when scanning the Raman line, for various control field powers and cell temperatures. For this figure only, the polarizations of the control field and probe beams were chosen so that they maximize the effect. Pc is the control beam power. (Modified from [25]). Click here to view larger image.

Discussion

A necessary condition for high memory efficiency is a high OD [30]. The OD of Λ-GEM is proportional to the Raman factor Ω_c^2/Δ^2, where Ω_c is the coupling field Rabi frequency and Δ is the Raman detuning from the excited state. The spontaneous Raman scattering rate is also proportional to the Raman factor and there is therefore a trade-off between achieving high absorption and low scattering losses. To find the optimum settings for the control field power, detuning and gas temperature we use an iterative process. The scattering losses can be mitigated to some extent by switching off the control beam during storage, after the pulse is fully absorbed. Optical depth is also affected by the internal state of the atoms. Ideally we would like to have as many atoms as possible in the F=1 hyperfine level to increase the absorption of the probe. The control beam also plays a role here as it acts to pump atoms from the F=2 to F=1 levels. This is not very efficient, due to the detuning, but the control beam is powerful and can be left on for long periods of time between pulse storage experiments. The width of the Raman line in our experiment is around 100 kHz, which is mostly a result of power broadening caused by the control field. This almost corresponds to the rate at which atoms are pumped from the F = 2 to the F = 1 hyperfine state. However there will be some population left on mf = 2 (or -2 depending on the sign of the circular polarization) of hyperfine level F = 2 due to the lack of allowed optical transitions.

The OD will also depend strongly on the temperature of the cell, which determines the number of atoms in the gas phase. We use a temperature of around 78 °C, measured at the center of the cell. We noticed that in our cell, increasing the temperature beyond 85 °C can result in some absorption of the control field as well as some incoherent absorption of the probe signal. The heater is switched off during the experimental run to avoid disturbing the magnetic field inside the cell.

Polarizations of both probe and control fields also play a crucial role in the absorption efficiency of the memory. The D1 transition line of 87Rb has two hyperfine excited states with a total of 8 Zeeman sublevels. In principle, the choice of identical circular polarizations for both the probe and the control fields ensures that they only interact with the excited state level mf = 2 (or -2), F' = 2. The linear or elliptical polarizations of the laser fields give rise to Raman coupling via other Zeeman sublevels of F' = 1, 2. This will result in broadening and asymmetry in the Raman line shape, due to the different coupling constants and ac Stark shifts of the various transitions. Unfortunately, identically circular polarized probe and control fields prepared before the memory can experience different polarization self-rotations as they propagate through the memory. This effect is more pronounced in high OD media, which we have in our experiment. This means that fine-tuning of probe and control beam polarization is needed to counteract the impact of self-rotation.

To further complicate matters, a degenerate four-wave mixing (FWM) process can sometimes be seen when working with large OD [25]. This can cause amplification and consequently introduce noise to the output state of the memory. In particular, when linear polarization is used for both the control and probe beams, the FWM effect can be greatly enhanced due to the Raman excitation through multiple excited states. The conditions under which the FWM process is either enhanced or suppressed in our system are summarized in Ref [25]. The impact of FWM can be mitigated

by, again, fine-tuning the polarization of the probe and control beams. In this way, FWM processes can be reduced to the point that they do not add noise to the recalled light [23]. With respect to FWM, it is worth noting that both cavities play an important role in suppressing the -6.8 GHz sideband generated by the Fiber-EOM that would otherwise seed the FWM process.

Both self-rotation and FWM affect the shape of the broadened Raman line. After fine-tuning, one can achieve a quite symmetric, roughly rectangular shaped absorption feature as shown in **Figure 5**. This contrasts with the case shown in **Figure 7** where polarizations were chosen to demonstrate the impact of FWM. Here the Raman feature is highly asymmetric.

As mentioned previously, a natural abundance Rb cell was used to filter the control beam and pass the probe beam to the detection section. Due to the high temperature of this cell, we noticed that air currents around the cell windows cause variation in the fringe visibility of the heterodyne detection, resulting in fluctuations of the signal. This effect has been minimized by implementing the heterodyne detection immediately after the filtering cell and reducing the air currents around the cell windows using appropriate oven design. We observed a probe loss of around 30% through the filtering cell, due to Fresnel reflections from the windows and to the absorption by ^{87}Rb atoms in the filtering cell. This loss can potentially be reduced by using antireflection coatings on the cell windows and using pure ^{85}Rb instead of a natural mixture of Rb.

In a warm vapor cell, diffusion is one of the main limitations to the storage time. After absorbing light, atoms can diffuse out of the coherent region, thus partially erasing the stored information. Adding a buffer gas (0.5 Torr Kr, in our experiment) reduces the effect of diffusion to some extent. Too much buffer gas, however, will increase collisional broadening [31]. This increases decoherence and control field absorption, which reduces the efficiency of the pumping mentioned above. Another way to reduce the effect of transverse diffusion is to increase the interaction volume by enlarging the transverse profiles of the probe and control fields. This approach will eventually be limited by inelastic collisions with the cell walls. In this case, the cell walls may be coated with antirelaxation materials [32, 33], to provide elastic collisions on the walls and therefore enhance the atomic coherence time. By minimizing the inelastic wall collision using proper wall coatings and increasing the laser beam size to almost cover the cell cross section, one would expect minimal effects from the transverse diffusion on the storage time. Longitudinal diffusion might then become the dominant decoherence effect at long storage times. Longitudinal diffusion causes the atoms to experience different magnetic field strengths during storage time that can result in reduced rephasing efficiency. One way to control longitudinal diffusion would be to use a cold atomic ensemble, such as atoms that have been cooled in a Magneto-Optic Trap (MOT). That, however, requires a whole new layer of experimental complexity involved in controlling cold atomic cloud. This is a system we are currently evaluating in our laboratory [36].

Disclosures

The authors declare that they have no competing financial interests.

Acknowledgements

The research is supported by the Australian Research Council Centre of Excellence for Quantum Computation and Communication Technology, project number CE110001027.

References

1. Knill, E., Laflamme, R., and Milburn, G. J. A scheme for efficient quantum computation with linear optics. *Nature*. **409**, 46-52 (2001).
2. Sangouard, N., Simon, C., De Riedmatten, H., and Gisin, N. Quantum repeaters based on atomic ensembles and linear optics. *Rev. of Mod. Phys.* **83**, 33-80 (2011).
3. Lvovsky, A. I., Sanders, B. C., and Tittel, W. Optical quantum memory. *Nat. Pho.* **3**, 706 (2009).
4. Fleischhauer, M., and Lukin, M. D. Dark-State Polaritons in Electromagnetically Induced Transparency. *Phys. Rev. Let.* **84**, 5094 (2000).
5. Afzelius, M., Simon, C., De Riedmatten, H., and Gisin, N. Multi-Mode Quantum Memory based on Atomic Frequency Combs. *Phys. Rev. A*. **79**, 052329 (2009).
6. Clausen, C., *et al.* Quantum storage of photonic entanglement in a crystal. *Nature*. **469**, 508 (2011).
7. Saglamyurek, E., *et al.* Broadband waveguide quantum memory for entangled photons. *Nature*. **469**, 512 (2011).
8. Boyer, V., McCormick, C. F., Arimondo, E., and Lett, P. D. Ultraslow Propagation of Matched Pulses by Four-Wave Mixing in an Atomic Vapor. *Phys. Rev. Let.* **99**, 143601 (2007).
9. Reim, K. F., Michelberger, P., Lee, K. C., Nunn, J., Langford, N. K., and Walmsley, I. A. Single-Photon- Level Quantum Memory at Room Temperature. *Phys. Rev. Let.* **107**, 053603-053604 (2011).
10. Jensen, K., *et al.* Quantum memory for entangled continuous-variable states. *Nature Physics*. **7**, 13 (2010).
11. Moiseev, S., and Kröll, S. Complete reconstruction of the quantum state of a single-photon wave packet absorbed by a Doppler-broadened transition. *Phys. Rev. Let.* **87**, 173601 (2001).
12. Moiseev, S. A., Tarasov, V. F., and Ham, B. S. Quantum memory photon echo-like techniques in solids. *Jour. Opt. B-Quan. Semiclass. Opt.* **5**, S497 (2003).
13. Nilsson, M., and Kröll, S. Solid state quantum memory using complete absorption and re-emission of photons by tailored and externally controlled inhomogeneous absorption profiles. *Opt. Comm.* **247**, 393-403 (2005).
14. Kraus, B., Tittel, W., Gisin, N., Nilsson, M., Kröll, S., and Cirac, J. I. Quantum memory for nonstationary light fields based on controlled reversible inhomogeneous broadening. *Phys. Rev. A*. **73**, 020302(R) (2006).
15. Alexander, A., Longdell, J J., Sellars, M., and Manson, N. Photon echoes produced by switching electric fields. *Phys. Rev. Let.* **96**, 043602 (2006).
16. Sangouard, N., Simon, C., Afzelius, M., and Gisin, N. Analysis of a quantum memory for photons based on controlled reversible inhomogeneous broadening. *Phys. Rev. A* **75**, 032327 (2007).
17. Damon, V., Bonarota, M., Louchet-Chauvet, A., Chaneliere, T., and Le Gouët, J.-L. Revival of silenced echo and quantum memory for light. *New Jour. of Phys.* **13**, 093031 (2011).

18. Hétet, G., Longdell, J. J., Alexander, A. L., Lam, P. K., and Sellars, M. J. Electro-Optic Quantum Memory for Light Using Two-Level Atoms. *Phys. Rev. Let.* **100**, 023601 (2008).
19. Hedges, M. P., Longdell, J. J., Li, Y., and Sellars, M. J. Efficient quantum memory for light. *Nature*. **465**, 1052-1056 (2010).
20. Hétet, G., Hosseini, M., Sparkes, B. M., Oblak, D., Lam, P. K., and Buchler, B. C. Photon echoes generated by reversing magnetic field gradients in a rubidium vapor. *Opt. Let.* **33**, 2323 (2008).
21. Hosseini, M., Sparkes, B. M., Hétet, G., Longdell, J. J., Lam, P. K., and Buchler, B. C. Coherent optical pulse sequencer for quantum applications. *Nature*. **461**, 241-245 (2009).
22. Hosseini, M., Sparkes, B. M., Campbell, G., Lam, P. K., and Buchler, B. C. High efficiency coherent optical memory with warm rubidium vapour. *Nat. Comm.* **2**, 174 (2011).
23. Hosseini, M., Campbell, G., Sparkes, B. M., Lam, P. K., and Buchler, B. C. Unconditional room-temperature quantum memory. *Nat. Phys.* **7**, 794-798 (2011).
24. Hosseini, M., Rebic, S., Sparkes, B. M., Twamley, J., Buchler, B. C., and Lam, P. K. Memory-enhanced noiseless cross-phase modulation. *Light: Sci. Apps.* **1**, e40 (2012).
25. Hosseini, M., Sparkes, B. M., Campbell, G., Lam, P. K., and Buchler, B. C. Storage and manipulation of light using a Raman gradient-echo process. *Jour. of Phys. B-Atomic Mol. and Opt. Phys.* **45**, 124004 (2012).
26. Barwood, G. P., Gill, P., and Rowley, W. R. C. Frequency measurements on optically narrowed Rb-stabilised laser diodes at 780 nm and 795 nm. *Appl. Phys. B*. **53**, 142-147 (1991).
27. Drever, R. W. P., *et al.* Laser phase and frequency stabilization using an optical resonator. *Appl. Phys. B-Photophys. and Laser Chem.* **31**, 97-105 (1983).
28. Sparkes, B. M., Chrzanowski, H. M., Parrain, D. P., Buchler, B. C., Lam, P. K., and Symul, T. A scalable, self-analyzing digital locking system for use on quantum optics experiments. *Rev. of Sci. Instr.* **82**, 075113 (2011).
29. Sparkes, B. M., *et al.* Precision Spectral Manipulation: A Demonstration Using a Coherent Optical Memory. *Phys. Rev.* X **2**, 021011 (2012).
30. Gorshkov, A. V., Andre, A., Fleischhauer, M., Sorensen, A. S., and Lukin, M. Universal approach to optimal photon storage in atomic media. *Phys. Rev. Let.* **98**, 123601 (2007).
31. Erhard, M., and Helm, H. Buffer-gas effects on dark resonances: Theory and experiment. *Phys. Rev. A*. **63**, 043813 (2001).
32. Balabas, M. V., *et al.* High quality anti-relaxation coating material for alkali atom vapor cells. *Opt. Expr.* **18**, 5825-5830 (2010).
33. Balabas, M. V., Karaulanov, T., Ledbetter, M. P., and Budker, D. Polarized alkali-metal vapor with minutelong transverse spin-relaxation time. *Phys. Rev. Let.* **105**, 070801 (2010).
34. Buchler, B. C., Hosseini, M., Hétet, G., Sparkes, B. M., and Lam, P. K. Precision spectral manipulation of optical pulses using a coherent photon echo memory, *Opt. Let.* **35**, 1091-1093 (2010).
35. Higginbottom, D. B. *Spatial Multimode Storage in a Gradient Echo Memory.* Honors thesis, Australian National University (2012).
36. Sparkes, B. M., *et al.* Gradient echo memory in an ultra-high optical depth cold atomic ensemble. *arXiv*. (2012).